Superstructure formation at the metal-insulator transition in $R\mathrm{BaCo_2O_{5.5}}$ (R=Nd,Tb) as seen from reciprocal space mapping

D. Chernyshov,[1] V. Dmitriev,[1] E. Pomjakushina,[2,3] K. Conder,[2] M. Stingaciu,[2] V. Pomjakushin,[3] A. Podlesnyak,[4,*] A. A. Taskin,[5,6] and Y. Ando[6]

[1]*Swiss-Norwegian Beam Lines, European Synchrotron Radiation Facility, BP220, 38043 Grenoble, France*

[2]*Laboratory for Developments and Methods, Paul Scherrer Institut, CH-5232 Villigen PSI, Switzerland*

[3]*Laboratory for Neutron Scattering, ETH Zurich & Paul Scherrer Institut, CH-5232 Villigen PSI, Switzerland*

[4]*Hahn-Meitner-Institut Berlin, Glienicker Straße 100, Berlin 14109, Germany*

[5]*Central Research Institute of Electric Power Industry, Komae, Tokyo 201-8511, Japan*

[6]*Institute of Scientific and Industrial Research, Osaka University, Ibaraki, Osaka 567-0047, Japan*

(Received 18 March 2008; revised manuscript received 7 May 2008; published 10 July 2008)

Single crystal synchrotron x-ray diffraction study has been performed on the layered perovskites $R\mathrm{BaCo_2O_{\sim 5.5}}$ (R=Tb,Nd) over a wide temperature range $100<T<375$ K. By means of reciprocal space mapping and symmetry analysis, it is shown that the first-order structural transition, accompanied by a metal-insulator transition, turns out to be a $Pmmm(a_c\times 2a_c\times 2a_c)\leftrightarrow Pmma(2a_c\times 2a_c\times 2a_c)$ transformation. The detailed structural analysis shows that all four different Co^{3+} ions possible within the space-group *Pmma* have different oxygen polyhedron distortions, thus, indicating ordering of different spin states.

DOI: 10.1103/PhysRevB.78.024105 PACS number(s): 61.05.C−, 61.50.Ks, 61.66.Fn

I. INTRODUCTION

In $R\mathrm{BaCo_2O_{5+\delta}}$ (R=rare earth element, $\delta\approx 0.5$), cobalt ions are coordinated by oxygen, forming square pyramids and octahedra.[1] Depending on the ligand field, Co^{3+} ions can be found in the low spin (LS, t_{2g}^6, $S=0$), intermediate spin (IS, $t_{2g}^5e_g^1$, $S=1$), or high spin (HS, $t_{2g}^4e_g^2$, $S=2$) state.[1] Providing that the energy difference between these states is small, $\sim k_BT$, different electronic and vibrational degeneracies may lead, via the entropy contribution, to a temperature induced spin-state conversion.[2] A change in the spin state of Co^{3+} is linked to macroscopic properties of the compound, such as conductivity and magnetism, and is probably related to the metal-insulating transition (MIT) observed in $R\mathrm{BaCo_2O_{5.5}}$. However, a microscopic picture of the process involves ordering of spin and orbital states, which is complex and not yet completely uncovered. One of the issues we address here is an ordering of the spin state of Co^{3+}, as manifested in the formation of superstructures. Corresponding superstructure reflections can be traced in a diffraction experiment as a function of external parameters.[3]

Superstructures reported so far are conveniently classified as multiplied periodicity of the primitive cubic perovskite, $a_c\times a_c\times a_c$. For $R\mathrm{BaCo_2O_{5.5}}$ with a disordered mixture of five and six coordinated Co ions involving a disorder of oxygen atoms, the crystal structure has $a_c\times a_c\times 2a_c$ $P4/mmm$ tetragonal symmetry, as revealed by neutron powder diffraction for $\mathrm{PrBaCo_2O_{5.5}}$ at $T=776$ K.[4] At room temperature, this compound shows an $a_c\times 2a_c\times 2a_c$ *Pmmm* orthorhombic structure.[4,5] Other powder-diffraction data for the same compound were interpreted in favor of an $a_c\times a_c\times 2a_c$ *Pmmm* space group.[6] For the $R=$ Nd analog, a similar $a_c\times a_c\times 2a_c$ structure has been observed in a powder-diffraction experiment[7] while neutron single-crystal data indicate $a_c\times 2a_c\times 2a_c$ periodicity[8] and space-group *Pmmm* is suggested for both data sets. For Gd-based cobaltite, an $a_c\times 2a_c\times 2a_c$ *Pmmm* structure was found to be consistent with synchrotron and neutron powder data[9] but $2a_c\times 2a_c\times 2a_c$ *Pmma* symmetry has been observed in a single-crystal x-ray diffraction experiment.[10] A set of $a_c\times a_c\times 2a_c$, $a_c\times 2a_c\times 2a_c$, and $2a_c\times 2a_c\times 2a_c$ structures were proposed on the basis of neutron powder data for $\mathrm{TbBaCo_2O_{5+\delta}}$.[3] It is also worth noting that a slight deviation of the oxygen content may lead to ordering of oxygen vacancies. Superstructure reflections corresponding to a nearly tripling of both the a and b axes have been observed for $\mathrm{TbBaCo_2O_{5+\delta}}$.[11] Even from this short and incomplete survey, it is clear that, despite a volume of experimental information, coherence is still lacking.

Bragg intensities indicating multiplication of the unit cell are usually several orders of magnitude weaker than the main reflections for both neutron and x-ray diffractions.[10] However, those weak reflections indicate the change in the symmetry that is concomitant with the change in the magnetic and spectroscopic properties, as illustrated by controversial interpretations of magnetic data for $R\mathrm{BaCo_2O_{5.5}}$.[3,12–14] Superstructure reflections manifesting ordering of different Co states are hardly visible in powder-diffraction data. Local probes such as extended x-ray-absorption fine structure (EXAFS) or NMR provide information that was averaged over a number of independent sites having different spin/orbital states. Single crystal measurements with point detectors may uncover superstructure reflections only if the reciprocal space between main Bragg reflections is scanned; this is a time consuming procedure. At variance with those methods, mapping of reciprocal space with the help of area detectors cannot overlook superstructure reflection, and, being combined with synchrotron radiation, allows fast and reliable data collection.

In this report, we use reciprocal space mapping with an area detector in order to obtain reliable data on weak diffraction features in cobaltites. These techniques have the advantage over previous diffraction studies due to the fact that any superstructure reflections cannot be missed, provided that ex-

posure time is sufficiently long. Mapping of reciprocal space has actively been used to measure weak diffraction features such as diffuse scattering in many compounds[15] but, as far as we are aware of, it has not yet been applied for studying superstructures in the rare-earth cobaltites.

The present single-crystal diffraction experiments are focused on $NdBaCo_2O_{5.5}$ and $TbBaCo_2O_{5.48}$. We present and discuss experimental information on the appearance of superstructure reflections and their temperature dependencies. We also show the results of a structural analysis for $NdBaCo_2O_{5.5}$ and illustrate that the corresponding powder-diffraction measurements could easily overlook the correct structure. A symmetry analysis bracketing the observed phase transitions in the framework of a rigorous, model free phenomenological scheme is also given.

II. SAMPLES

High-quality $TbBaCo_2O_{5+\delta}$ and $NdBaCo_2O_{5+\delta}$ single crystals have been grown by the floating zone technique, using infrared image furnaces with four (FZ-T-10000-H-IV-VP-PC, Crystal System Corp., Japan) and two (NEC Machinery SC E-15HD, Japan) halogen lamps as a heat source, respectively. Polycrystalline feed rods used for the crystal growth were prepared by the conventional solid-state method: The stoichiometric mixture of Tb_4O_7, Co_3O_4, and $BaCO_3$ powders with purity of 99.99% (Nd_2O_3, CoO, and $BaCO_3$ in the case of $NdBaCo_2O_{5+\delta}$) were calcinated/sintered at 900–1200 °C in air for at least 100 h with several intermediate grindings. The purity of the synthesized phases was confirmed using a conventional x-ray diffractometer. Rods of 6–8 mm in diameter and 60–100 mm in length formed from isostatically pressed powder were finally sintered at 1300 °C for 30 h to make them hard and dense. The crystal growth was performed at a constant rate of 0.5 mm/h with both the feed and seed rods rotating at about 15 rpm in opposite directions to ensure homogeneity of the melt. The 5.5-bar pressure of oxygen and argon mixture was applied during the growth of $TbBaCo_2O_{5+\delta}$ while $NdBaCo_2O_{5+\delta}$, in which the difference between the ionic radii of Ba and Nd is less pronounced, was grown in the atmosphere of pure argon in order to prevent a possible disorder among Ba and Nd positions by reducing the oxygen content of the compound during the growth.

A few crystals of $TbBaCo_2O_{5+\delta}$ were separated from the as-grown chunk and annealed in the oxygen atmosphere (1 bar, 600 °C) together with the as-prepared powder. Both the powder and the crystals have shown very pronounced differential scanning calorimetry (DSC) peak corresponding to the MIT at the same temperature (336 K), suggesting that they have identical oxygen content,[16] which was measured by iodometric titration[17] in the powder sample and was found to be 5.48 ± 0.01.

Oxygen content in $NdBaCo_2O_{5+\delta}$ was determined with the help of the thermogravimetric analysis (TGA) and it was tuned to the value of 5.50 with an accuracy better than ± 0.002, using the annealing technique that was initially developed for obtaining $GdBaCo_2O_{5.5}$ single crystals, as described in detail in Ref. 18. Pristine orthorhombic $RBaCo_2O_{5.5}$ crystals are usually heavily twinned. In order to obtain single-domain orthorhombic crystals for diffraction experiments, the detwinning of $NdBaCo_2O_{5.5}$ samples was performed at an elevated temperature (~220 °C), which was high enough for the movement of twin domain boundaries under applied pressure but still low enough for the bulk oxygen diffusion and oxygen exchange with ambient atmosphere. The uniaxial pressure of 0.15–0.20 GPa applied along the $a(b)$ axis was enough for the twin boundary motion, which was controlled by a polarized-light optical microscope. Detwinned crystals were slowly cooled down under the pressure. For large samples, this procedure was repeated several times. The remaining fraction of misoriented domains in $NdBaCo_2O_{5.5}$ samples, which was estimated from the magnetization anisotropy measured along the a and b axes, did not exceed 3%. There were, therefore, two single crystals used for the synchrotron diffraction experiments: twinned $TbBaCo_2O_{5.48}$ and detwinned $NdBaCo_2O_{5.5}$.

III. EXPERIMENT

Diffraction data were collected at the Swiss-Norwegian Beam Lines (BM1A) of the European Synchrotron Radiation Facility (ESRF, Grenoble, France) using an image plate detector MAR345 and a monochromatic beam with wavelength $\lambda = 0.71$ Å, and at the six-circle KUMA6 diffractometer equipped with an ONYX charge coupled device (CCD) detector with $\lambda = 0.72$ Å. The temperature was controlled with Oxford Cryostream 700+. Layers of reciprocal space have been reconstructed with help of the CRYSALIS software.[19] The same software has been used for data reduction. For detwinned $NdBaCo_2O_{5.5}$, it was possible to collect a full-sphere data set of Bragg intensities, including those from the superstructure at $T = 100$ K. The corresponding crystal structure was solved with SHELXS and refined with SHELX.[20] Simulation and analysis of powder data were done with the FULLPROF software.[21] The temperature dependence of selected reflections was monitored with broad (4°) repeatedly collected φ scans during cooling/heating process using the ONYX CCD detector. The width of the scan was selected to assure that reflections of interest do not leave the scanned zone of reciprocal space due to the temperature variation of the orientation matrix.

IV. RESULTS

Single crystals of rare-earth cobaltites are usually twinned by changing orthogonal a and b axes; corresponding twin matrix is [010 100 00–1]. Having access to a full-sphere distribution of diffracted intensities, this problem can effectively be reduced. Portions of reciprocal layers for $NdBaCo_2O_{5.5}$ at 100 K (Fig. 1) show how a twinned single-crystal space-group $Pmmm$ with periodicity $a_c \times 2a_c \times 2a_c$, often found in powder-diffraction studies,[4,8,9] can safely be distinguished from $Pmma$ ($2a_c \times 2a_c \times 2a_c$). For a twinned crystal, a phase transition between $Pmma$ and $Pmmm$ can therefore be observed from the temperature dependence of superstructure reflections with the h and k both odd, $l \neq 0$. These superstructure reflections have to disappear above the

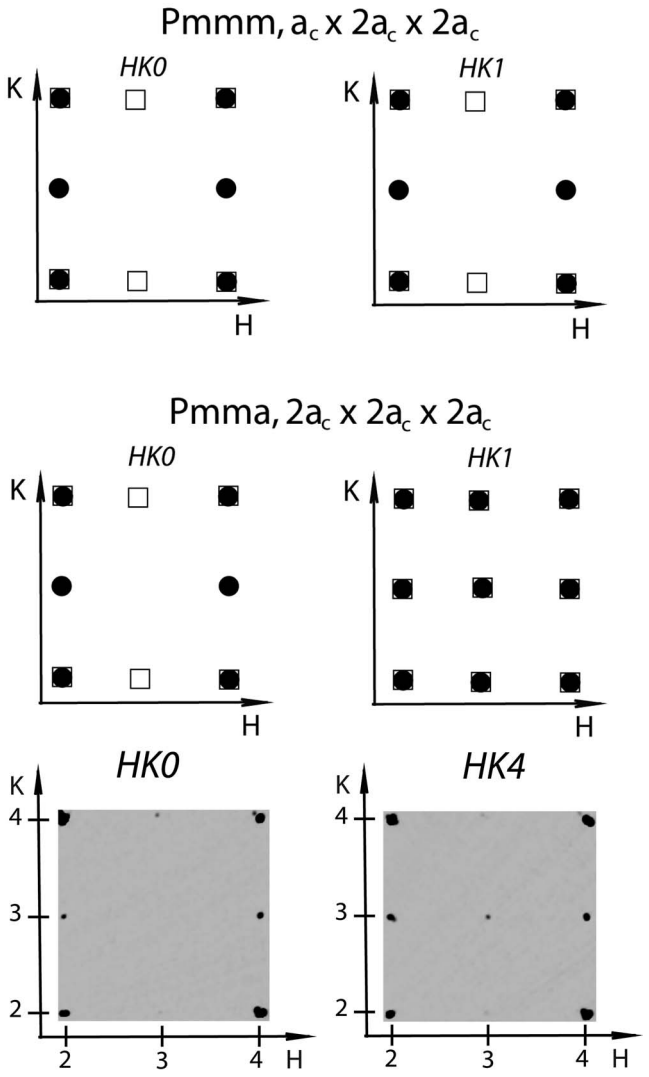

FIG. 1. Twinning patterns in reciprocal space for *Pmmm* ($a_c \times 2a_c \times 2a_c$) and *Pmma* ($2a_c \times 2a_c \times 2a_c$) structures. Filled cycles and empty boxes correspond to different twin components. Two structures can be distinguished from *hkl* ($l \neq 0$) layers while *hk*0 layers look the same. Fragments of reciprocal layers reconstructed from the experiment are shown for $NdBaCo_2O_{5.5}$ at 100 K at the bottom panel.

transition temperature. The reflections of the second type with only *h* or *k* odd overlap with the main reflections from the second twin component; a change of intensity of this reflections can be used to follow the transition. A first-order transition at $T \sim 350$ K thus follows from Fig. 2 for the Nd-based compound. Above this temperature, coinciding with the temperature for a metal-insulator transition, all observed reflections correspond to the *Pmmm* ($a_c \times 2a_c \times 2a_c$) twinned structure. A detailed inspection of reciprocal space for $NdBaCo_2O_{5.5}$ at temperatures down to 100 K does not reveal superstructure reflections corresponding to $2a_c \times 2a_c \times 4a_c$ periodicity, as reported for the Dy analog.[22] The ratio of the intensities of main and superstructure reflections for $NdBaCo_2O_{5.5}$ at 100 K was within the dynamic range of the MAR345 image plate detector and we have collected a single-crystal data set having only few strong reflections

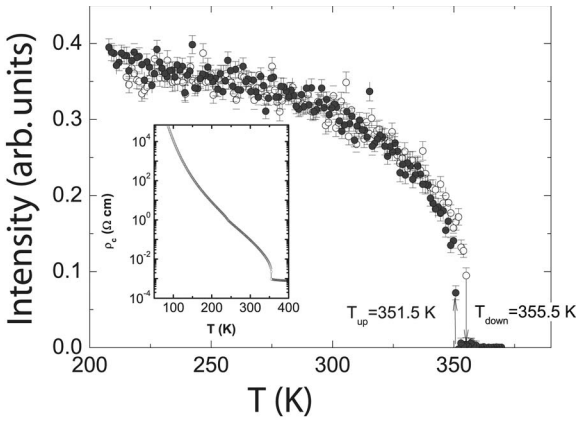

FIG. 2. Temperature dependence of the intensity of the $\bar{1}18$ Bragg reflection for $NdBaCo_2O_{5.5}$ measured on cooling and heating modes. Inset: temperature dependence of the resistivity, which demonstrates that the metal-insulating transition and the appearance of superstructure reflections coincide.

overexposed (Table I). However, since the intensity of superstructure reflections is generally much lower, the refinement results, as expected, in a relatively high value of weighted residuals. The data correspond to the *Pmma* ($2a_c \times 2a_c \times 2a_c$) structure (we use this unit cell for indexing of Bragg reflections throughout the paper) with four different cobalt ions: two in pyramids and two in octahedral coordinations. All of them have different size and distortion pat-

TABLE I. Crystal data and structure refinement for $NdBaCo_2O_{5.5}$ at $T=100$ K.

Empirical formula	$BaCo_2NdO_{5.50}$
Temperature	100(1) K
Wavelength	0.72184 Å
Crystal system	*mmm*
Space group	*Pmma*
Unit cell dimensions	$a=7.7815(10)$Å $\alpha=90°$
	$b=7.8353(6)$Å $\beta=90°$
	$c=7.5595(10)$Å $\gamma=90°$
Volume	460.91(9)Å^3
Z	4
Absorption coefficient	26.512 mm^{-1}
Θ range for data collection	2.64°–27.61°
Index ranges	$-9 \leq h \leq 9$,
	$-10 \leq k \leq 10$,
	$-9 \leq l \leq 9$
Reflections collected	2872
Independent reflections	575 [$R_i=0.0510$]
Completeness to $\Theta=27.61°$	94.2%
Refinement method	Full-matrix least squares on F^2
Data/restraints/parameters	575/0/65
Goodness of fit on F^2	1.132
Final *R* indices [$I>2\sigma(I)$]	$R_1=0.0453$, $wR_2=0.1555$
R indices (all data)	$R_1=0.0553$, $wR_2=0.1761$

TABLE II. Atomic coordinates ($\times 10^4$) and equivalent isotropic displacement parameters ($Å^2 \times 10^3$) for $NdBaCo_2O_{5.5}$. U(eq) is defined as one third of the trace of the orthogonalized U^{ij} tensor.

	x	*y*	*z*	U(eq)
Nd(1)	0	2712(2)	5000	7(1)
Ba(1)	0	2515(1)	0	7(1)
Co(1)	2500	0	2508(2)	7(1)
Co(2)	2500	0	7466(2)	9(1)
Co(3)	2500	5000	2538(2)	6(1)
Co(4)	2500	5000	7528(2)	7(1)
O(1)	2500	0	−18(12)	16(3)
O(2)	2500	5000	9988(11)	8(3)
O(3)	2500	5000	5008(13)	18(4)
O(4)	138(9)	0	3071(12)	13(2)
O(5)	51(9)	5000	2692(12)	12(3)
O(61)	2500	2508(11)	2818(13)	11(2)
O(62)	2500	2298(10)	7052(13)	10(2)

terns of the coordination polyhedron. The refined structural parameters are summarized in Tables II and III. These data were used as an initial model to refine x-ray powder-diffraction data (see Fig. 3) by the Rietveld method. Analysis clearly shows that, at variance with the single-crystal data, the powder pattern can be reproduced equally well within both *Pmma* ($2a_c \times 2a_c \times 2a_c$) and *Pmmm* ($a_c \times 2a_c \times 2a_c$) models (see also Refs. 6, 8–14, and 23). The intensity of the additional superstructure satellites ($l \neq 0, h, k) = 2n+1$, [e.g., (1 1 1), Fig. 3] is much smaller than the typical error bars given by the background. We found that the refinement of structure parameters from the powder patterns for *Pmma*($2a_c \times 2a_c \times 2a_c$) is not statistically relevant.

As compared with $NdBaCo_2O_{5.5}$, a single crystal of $TbBaCo_2O_{5.48}$ shows a similar first-order transition at $T \sim 336$ K corresponding to the change of symmetry from *Pmma* ($2a_c \times 2a_c \times 2a_c$) to *Pmmm* ($a_c \times 2a_c \times 2a_c$), as follows from the extinction of superstructure reflections with the *h* and *k* both odd, $l \neq 0$ above the transition temperature. The temperature dependence of these reflections is very similar to that for $NdBaCo_2O_{5.5}$ except for the difference in transition temperature and hysteresis width. As it is noted before, the transition can also be seen from the temperature dependence of reflection affected by twinning; in this case we have observed nearly halving of the intensity (Fig. 4).

There are, however, some well visible differences between the Tb- and Nd-based analogs. First, at all temperatures, additional weak reflections corresponding to a nearly tripling of both the *a* and *b* axes were observed (Fig. 5 top) similar to those observed before.[8] Superstructure reflections nearly tripling the *a* and *b* axes slightly decrease in intensity on heating without any peculiarities in their temperature dependence. Contrary to $NdBaCo_2O_{5.5}$ and similar to $DyBaCo_2O_{5.5}$,[22] a new set of superstructure reflections corresponding to $2a_c \times 2a_c \times 4a_c$ is clearly observed below 180 K (Fig. 5). The only reflection condition observed is $l=2n$ for 00*l*. Among space groups generated by irreducible representations at the *Z* point of the Brillouin zone for *Pmma* space group,[24] only twinned *Pmca* (no. 57) or *Pcma* (no. 55) structure would give the same pattern. This conclusion, however, has to be taken with a grain of salt since, according to Ref. 22, the transition can be of a first order, and thus, lack of direct group-subgroup relations cannot be completely excluded. Moreover, one has to keep in mind that the real crystal structure of $TbBaCo_2O_{5+\delta}$ is, by far, more complex and, accounting for the ordering of vacancies, has $6a_c \times 6a_c \times 4a_c$ periodicity in the low-temperature phase.

TABLE III. Selected bond lengths [Å]. Symmetry transformations used to generate equivalent atoms are the following: #1 $-x,-y+1,-z+1$; #3 $-x,-y,-z+1$; #4 $x,y,z-1$; #8 $-x+1/2,-y,z$; #10 $x+1/2,y,-z+1$; #11 $x,y,z+1$; #13 $-x+1/2,-y+1,z$.

Co(1)-O(4)#8	1.886(7)
Co(1)-O(4)	1.886(7)
Co(1)-O(1)	1.909(9)
Co(1)-O(61)#8	1.979(8)
Co(1)-O(61)	1.979(8)
Co(2)-O(62)#8	1.827(8)
Co(2)-O(62)	1.827(8)
Co(2)-O(1)#11	1.901(9)
Co(2)-O(4)#3	2.093(8)
Co(2)-O(4)#10	2.093(8)
Co(3)-O(3)	1.867(10)
Co(3)-O(5)#13	1.910(7)
Co(3)-O(5)	1.910(7)
Co(3)-O(2)#4	1.928(8)
Co(3)-O(61)	1.964(8)
Co(3)-O(61)#13	1.964(8)
Co(4)-O(2)	1.860(8)
Co(4)-O(3)	1.905(10)
Co(4)-O(5)#1	1.992(7)
Co(4)-O(5)#10	1.992(7)
Co(4)-O(62)	2.148(8)
Co(4)-O(62)#13	2.148(8)

V. DISCUSSION AND CONCLUSIONS

Both cobaltites $NdBaCo_2O_{5.5}$ and $TbBaCo_2O_{5.48}$ show a $Pmmm(a_c \times 2a_c \times 2a_c) \leftrightarrow Pmma(2a_c \times 2a_c \times 2a_c)$ phase transition. A tetragonal structure with $P4/mmm$ ($a_c \times a_c \times 2a_c$) symmetry is expected to appear on heating, as it has been seen for $PrBaCo_2O_{5.5}$,[4] due to disordering of oxygen atoms between pyramids and octahedra. One can also see that disordering of rare-earth and barium atoms would bring the tetragonal structure into the parent perovskite $Pm3m$ ($a_c \times a_c \times a_c$) structure. To parametrize this pathway, we use a procedure similar to that employed to compute the tables in Ref. 24. It gives straight conclusions on the transformation mechanisms, bringing a cubic perovskite structure

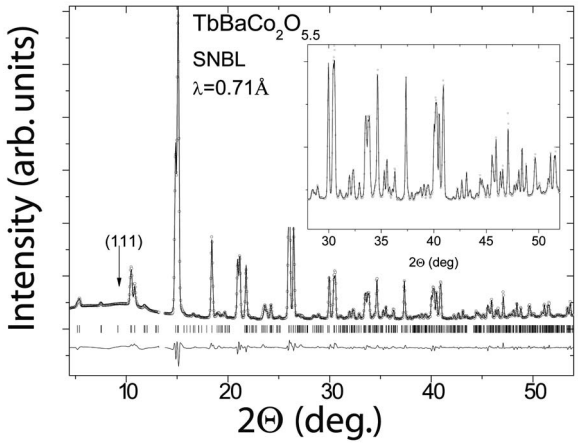

FIG. 3. Example of the Rietveld refinement pattern in the "ordered" structure model *Pmma* (see text). The inset shows a selected region in a zoom scale. Note that, in spite of the doubled unit cell for the *Pmma* model, the density of peaks is practically the same, as in the case of the *Pmmm* model, due to the extinctions caused by the *a*-gliding plane.

to the orthorhombic one observed in the cobaltite crystals at ambient conditions. A straightforward group-theoretical procedure starts from the cubic structure and enumerates its *stable low-symmetry phases*, thus allowing us to conclude that an orthorhombic phase belonging to the space-group *Pmmm* with a superstructure $a_c \times 2a_c \times 2a_c$ stems from a combined distortion of the parent structure by two order parameters (OPs) belonging to the point *X* (three-arms star $k^{(1)}=b_1/2$) of the primitive cubic Brillouin zone (BZ). The components of the first OP span the three-dimensional irreducible representation (IR) X_1.[25] Activity of different mechanisms (Table IV) indicates that the relevant mechanism includes ordering R/Ba ions randomly distributed in the position 1(*a*) of the cubic perovskite structure, as well as displacement of Co and O ions. This results in a virtual tetragonal structure $P4/mmm(a_c \times a_c \times 2a_c)$. The second OP, spanning IR X_4, establishes the order in the Co sublattice and transforms the parent structure into another tetragonal one $P4/mmm(a_c \times a_c \times 2a_c)$. Finally, both OPs, X_1 and X_4, induce ordering of the oxygen ions, which forms two types of oxygen polyhedra, pyramids and octahedra, coordinating, therefore, crystallographically different Co cations. Thus, one concludes on a combined, ordering, and displacive mechanism of the corresponding cubic-to-orthorhombic transformation. It is worth noting that a single component of each three-component OP becomes active in the *Pmmm* phase. Figure 6(a) summarizes the effect of the OPs distortion, bringing a perovskite structure to the *Pmmm* orthorhombic one of the cobaltite crystal.

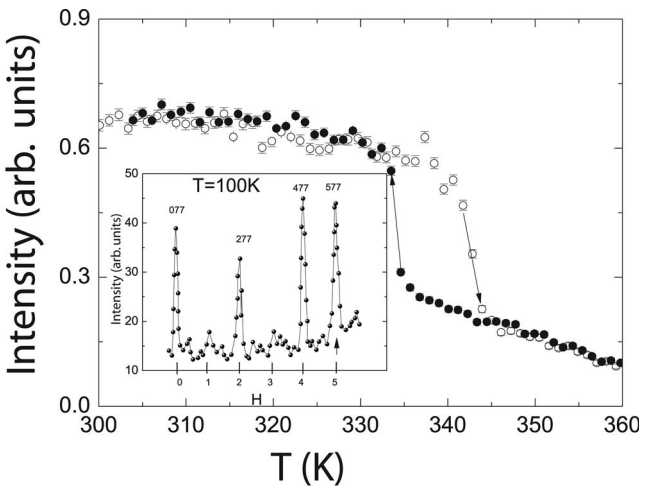

FIG. 4. Intensity of the twinned $5\bar{2}2$ reflection as a function of temperature for $TbBaCo_2O_{5.48}$. The inset shows a scan across *h* of the *hk*7 reciprocal layer for $TbBaCo_2O_{5.48}$ at $T=100$ K with the 577 reflection, which is forbidden in the *Pmmm* model.

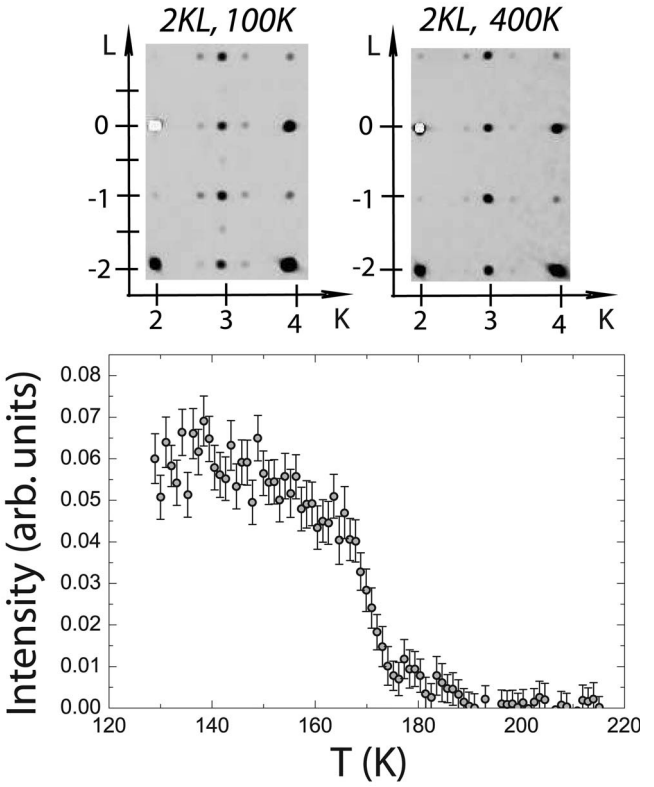

FIG. 5. Top: sections of 2*kl* reciprocal layers measured at 400 and 100 K with $TbBaCo_2O_{5.48}$ crystal. *k* and *l* indices are shown for $2a_c \times 2a_c \times 2a_c$ lattice. Bottom: temperature dependence of the $\bar{5}2\frac{3}{2}$ reflection for $TbBaCo_2O_{5.48}$.

Concerning the $Pmmm(a_c \times 2a_c \times 2a_c) \leftrightarrow Pmma(2a_c \times 2a_c \times 2a_c)$ phase transformation, the conclusion of the group-theoretical analysis is unambiguous as well. It predicts

TABLE IV. Permutation and mechanical representations for different positions of the space-group *Pm*3*m* in the *x* point of Brillouin zone.

Position: atom	Ordering	Displacements
1(a): Ba/R	X_1	X_4+X_{10}
1(b): Co	X_4	X_1+X_9
3(c): O	$X_1+X_4+X_8$	$X_1+X_4+X_6+2X_9+X_{10}$

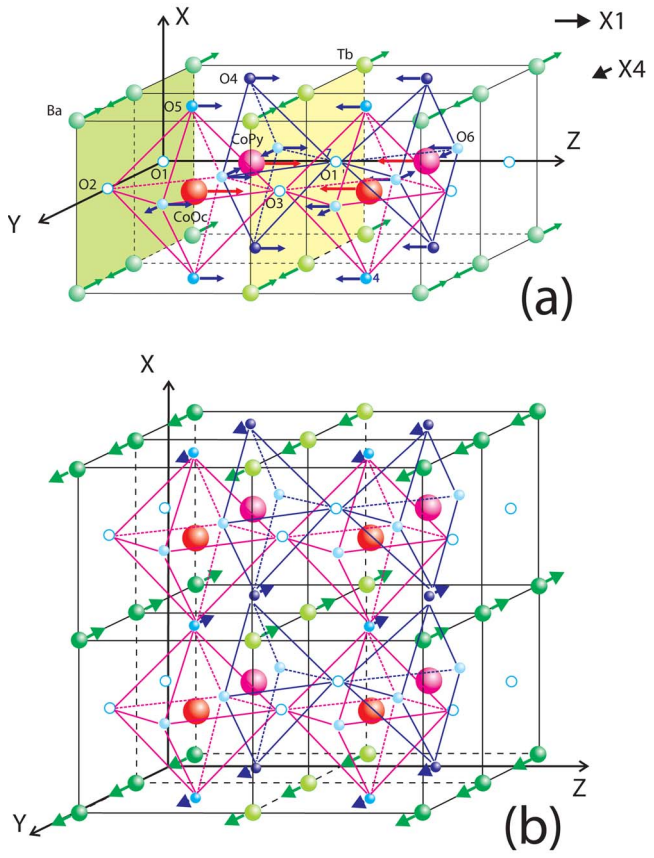

FIG. 6. (Color online) Eigenvectors for the atomic displacements forming the orthorhombic cobaltite structures: (a) X_1—shifts parallel to Z; X_4—parallel to Y, and (b) X_{10}.

the X_{10} phonon mode to be a destabilizing factor of the above transformation. Only single set of displacements, among six symmetry equivalent, distorts *Pmmm* $(a_c \times 2a_c \times 2a_c)$ structure; therefore establishing a new *Pmma* $(2a_c \times 2a_c \times 2a_c)$ superstructure. It is worth noting that the positions of R/Ba and oxygen ions but not the Co ones are affected by this distortion (see Table IV). Note that the change of the spin state of cobalt is mainly manifested in displacements of oxygen. Figure 6(b) shows the corresponding shift of the ions.

The present structural data are therefore coherent with the most general, symmetry-based analysis of the structure transformations in perovskite based cobaltite crystals. This parametrization of structural distortions does not tell which Co ions stay in which spin state. However, it clearly states that above the metal-insulator transition, there are two different Co ions in the unit cell located in pyramidal and octahedral coordinating polyhedrons while below there are four different Co ions. All four independent cobalt ions show different distortions of coordinating polyhedrons and that evidences, in agreement with resent magnetic studies for Tb (Ref. 3) and Ho (Ref. 26) analogs, an ordering of different spin states also for $NdBaCo_2O_{5.5}$. Thus, in contrast to the conclusions of Soda *et al.*,[14] it appears clearly that a *Pmmm*↔*Pmma* structural transition creating four different Co ions takes place *simultaneously* with MIT and surely should be taken into account in all models of metal-insulating, as well as magnetic, transitions of $RBaCo_2O_{5.5}$ that are related with the ordering of different Co states.

ACKNOWLEDGMENTS

Y.A. was supported by KAKENHI Contract No. 19674002. D.C. is grateful to Y. Filinchuk (Swiss-Norwegian Beam Lines) for numerous fruitful discussions on twinning problems. The authors thank V. Shirokov for offering to use his group-theoretical program package, and R. Feyerherm for careful reading of the manuscript and helpful discussions. Financial support by the Swiss National Science Foundation through Grant No. SCOPES IB7320-110859/1 and NCCR MaNEP project is gratefully acknowledged.

*Corresponding author.andrei.podlesnyak@hmi.de

[1] A. Podlesnyak, K. Conder, E. Pomjakushina, and A. Mirmelstein, in *Frontal Semiconductor Research*, edited by O. T. Chang (Nova Science, New York, 2006).
[2] S. Miyashita, Y. Konishi, H. Tokoro, M. Nishino, K. Boukheddaden, and F. Varret, Prog. Theor. Phys. **114**, 719 (2005).
[3] V. P. Plakhty, Y. P. Chernenkov, S. N. Barilo, A. Podlesnyak, E. Pomjakushina, E. V. Moskvin, and S. V. Gavrilov, Phys. Rev. B **71**, 214407 (2005).
[4] S. Streule *et al.*, Phys. Rev. B **73**, 094203 (2006).
[5] A. Maignan, C. Martin, D. Pelloquin, N. Nguyen, and B. Raveau, J. Solid State Chem. **142**, 247 (1999).
[6] S. Streule, A. Podlesnyak, M. Medarde, K. Conder, E. Pomjakushina, and J. Mesot, J. Phys.: Condens. Matter **17**, 3317 (2005).
[7] J. F. Mitchell, J. Burley, and S. Short, J. Appl. Phys. **93**, 7364 (2003).
[8] M. Soda, Y. Yasui, M. Ito, S. Iikubo, M. Sato, and K. Kakurai, J. Phys. Soc. Jpn. **73**, 2857 (2004).
[9] C. Frontera, J. L. García-Muñoz, A. E. Carrillo, M. A. G. Aranda, I. Margiolaki, and A. Caneiro, Phys. Rev. B **74**, 054406 (2006).
[10] Y. P. Chernenkov, V. P. Plakhty, V. I. Fedorov, S. N. Barilo, S. V. Shiryaev, and G. L. Bychkov, Phys. Rev. B **71**, 184105 (2005).
[11] M. Soda, Y. Yasui, T. Fujita, T. Miyashita, M. Sato, and K. Kakurai, J. Phys. Soc. Jpn. **72**, 1729 (2003).
[12] F. Fauth, E. Suard, V. Caignaert, and I. Mirebeau, Phys. Rev. B **66**, 184421 (2002).
[13] D. D. Khalyavin, Phys. Rev. B **72**, 134408 (2005).
[14] M. Soda, Y. Yasui, Y. Kobayashi, T. Fujita, M. Sato, and K. Kakurai, J. Phys. Soc. Jpn. **75**, 104708 (2006).
[15] T. R. Welberry and B. D. Butler, J. Appl. Crystallogr. **27**, 205 (1994).
[16] K. Conder, E. Pomjakushina, V. Pomjakushin, M. Stingaciu, S. Streule, and A. Podlesnyak, J. Phys.: Condens. Matter **17**, 5813 (2005).
[17] K. Conder, E. Pomjakushina, A. Soldatov, and E. Mitberg, Mater. Res. Bull. **40**, 257 (2005).

[18] A. A. Taskin, A. N. Lavrov, and Y. Ando, Phys. Rev. B **71**, 134414 (2005).
[19] CRYSALIS Software System, Ver. 1.171.31.4, Oxford-diffraction Ltd., Oxford (England), 2006.
[20] G. M. Sheldrick, *SHELXL97* (University of Göttingen, Göttingen, Germany, 1997).
[21] J. Rodríguez-Carvajal, Physica B (Amsterdam) **192**, 55 (1993).
[22] Y. Chernenkov, V. Plakhty, A. Gukasov, S. Barilo, S. Shiryaev, G. Bychkov, V. Hinkov, V. Fedorov, and V. Chekanov, Phys. Lett. A **365**, 166 (2007).
[23] E. Pomjakushina, K. Conder, and V. Pomjakushin, Phys. Rev. B **73**, 113105 (2006).
[24] H. T. Stokes and D. M. Hatch, *Isotropy Subgroups of the 230 Crystallographic Groups* (World Scientific, Singapore, 1988).
[25] We use the enumeration of irreducible representations according to O. V. Kovalev, *Irreducible Representations of the Space Groups* (Gordon and Breach, New York, 1965).
[26] J.-E. Jørgensen and L. Keller, Phys. Rev. B **77**, 024427 (2008).